MATERIALS SCIENCE

10.1126/sciadv.1600320

Stabilizing electrodeposition in elastic solid electrolytes containing immobilized anions

Mukul D. Tikekar,[1] Lynden A. Archer,[2]* Donald L. Koch[2]*

Ion transport–driven instabilities in electrodeposition of metals that lead to morphological instabilities and dendrites are receiving renewed attention because mitigation strategies are needed for improving rechargeability and safety of lithium batteries. The growth rate of these morphological instabilities can be slowed by immobilizing a fraction of anions within the electrolyte to reduce the electric field at the metal electrode. We analyze the role of elastic deformation of the solid electrolyte with immobilized anions and present theory combining the roles of separator elasticity and modified transport to evaluate the factors affecting the stability of planar deposition over a wide range of current densities. We find that stable electrodeposition can be easily achieved even at relatively high current densities in electrolytes/separators with moderate polymer-like mechanical moduli, provided a small fraction of anions are immobilized in the separator.

INTRODUCTION

Dendrite formation and growth are important factors limiting the commercialization of rechargeable lithium batteries that use metallic lithium as the anode. The other factor is that the high reactivity of lithium metal with most commonly used liquid electrolyte solvents continuously consumes electrolyte at the anode-electrolyte interface and in a parasitic cycle and this is exacerbated by rough or dendritic electrodeposition. Upon recharging a lithium metal battery (LMB), lithium deposits unevenly on the lithium anode, leading to the formation of dendrites, which can grow and short circuit the battery internally. Alternately, growing dendrites can break off, leading to electrically disconnected lithium, which degrades performance of the battery over time.

Although the lithium dendrite problem is of recent interest, it bears a physical resemblance to other historically well-known reaction-diffusion problems such as ramified electrodeposition (*1*, *2*), unstable solidification of binary alloys (*3*), branched growth of bacterial colonies (*4*), and surface roughening of epitaxial thin films (*5*). Rather, the lithium dendrite growth is regarded as a form of ramified electrodeposition, which is more colloquially used to refer to dendrite formation in aqueous solutions of transition metals such as copper, zinc, and silver.

Dendritic deposition typically progresses in three stages. In the first stage, microscopic seeds nucleate on the metal surface, acting as points of local deposition. In transition metals such as copper, zinc, and nickel, nucleation takes place because of depletion of the salt near the metal surface on polarization (*1*, *6*). Highly reactive metals such as lithium and sodium react parasitically with the electrolyte to form a thin passivation layer called the solid-electrolyte interphase (SEI) on the metal surface. Inhomogeneities in the SEI present as a result of its spontaneous formation are also a source of nucleation. Continual deposition on these nuclei leads to initiation of dendrites by growth of the seeds. The growth of the nuclei is driven by the transport of ions in deposition and resisted by thermodynamic factors such as surface tension of the metal-electrolyte interface, which favors a low-surface-area, flat and homogeneous deposition. On further deposition on the nuclei, the dendrites undergo accelerated growth to form macroscopic structures, which exhibit a variety of morphologies from moss-like aggregates at low current densities to thin needles at high current densities (*7*). These structures are mechanically strong enough to pierce through the separator and bridge the interelectrode gap, causing short circuits. This growth is highly nonlinear and unrestrained. Thus, dendritic deposition is difficult to control in the first nucleation and the final accelerated growth stages. It is therefore more effective to address the problem in the second stage, namely, growth of nuclei.

A number of studies have investigated the factors responsible for dendritic deposition. Both theory (*1*) and experiments (*2*) have effectively established that the primary mechanism behind dendrite growth is the preferential transport of ions to the dendrite tips. Models that examine these instabilities in charge transport primarily focus on factors that determine the initial growth of small perturbations of various shapes, such as hemispheres, cylinders, or sinusoids, to the metal surface. Studies based on Mullins-Sekerka–type stability analysis (*6*, *8*, *9*) favor the sinusoidal shape on account of its generalizability to several geometries and examine its growth under surface tension–mediated electrodeposition. The goal of these studies is to examine the relative competition of factors that govern dendrite growth, rather than predict the long-time morphology of the deposits. Typically, such analyses assume dilute solution theory to model transport in conventional salt electrolytes in liquid media, with surface tension as the only factor stabilizing the electrodeposition.

Solid and gel polymer electrolytes are regarded as viable alternatives to the conventional salt-in-liquid electrolytes, because they resist growth of dendrites by slowing the interfacial deformation (*10*, *11*). In addition, solid electrolytes are favored in battery applications due to their thermal and mechanical stability, while making batteries easier to process and handle and opening up the possibility of miniaturization. The solid structure also fulfills the role of a separator by physically separating the two electrodes. Monroe and Newman (*12*) examined the effect of elastic deformation of a solid separator on the interfacial kinetics at the electrode-electrolyte interface to model the growth of small sinusoidal perturbations to a metallic electrode. They deformed the separator-electrode interface and

[1]Sibley School of Mechanical and Aerospace Engineering, Cornell University, Ithaca, NY 14853, USA. [2]Robert Frederick Smith School of Chemical and Biomolecular Engineering, Cornell University, Ithaca, NY 14853, USA.
*Corresponding author. Email: laa25@cornell.edu (L.A.A.); dlk15@cornell.edu (D.L.K.)

obtained the pressure in the separator and electrode through linear elastic deformation theory. These calculations indicated that the perturbations decay with time if the separator shear modulus is greater than or equal to the shear modulus of the metal, which in the case of lithium is around 3.4 GPa at 25°C. However, such moduli are difficult to achieve in conventional solid polymer electrolytes without compromising ionic conductivity. Solid polymers or polymer-solvent gels that are conductive enough to support battery operation typically fall short of the desired modulus by three or more orders of magnitude. Ceramic electrolytes have also been actively investigated for their ability to comfortably meet this modulus requirement, but suffer from a variety of stubborn problems associated with their brittleness, poor processability, high cost, and low ionic conductivity at room temperature.

The experiments of Stone *et al.* (*13*) with polystyrene–block–polyethylene oxide block copolymer solid electrolytes provided partial support for the theoretical predictions of Monroe and Newman (*12*). Their research showed that symmetric lithium cells could be cycled for much longer durations by increasing the separator shear modulus. The total charge passed in the cycling was measured and plotted against the separator shear modulus. Extrapolation of the plots revealed that the total charge passed diverges at a separator shear modulus close to the theoretically predicted value given by Monroe and Newman (*12*). Several studies with a variety of solid polymer electrolytes such as cross-linked polymers (*14*, *15*) or polymer nanocomposites (*16*–*19*) later presented contradicting evidence, wherein symmetric lithium cells could be cycled for very long times even with low separator moduli (~1 MPa). It was also observed that the stability of the deposition depended strongly on current density, consistent with several other studies in liquids and gels (*20*–*23*) and in agreement with theoretical predictions (*6*, *8*, *9*). These observations cannot be explained by the Monroe and Newman analysis (*12*). This suggests the need for an analysis that incorporates the effect of both the separator mechanics and ion transport to determine the conditions for stabilizing electrodeposition.

Previously, we proposed a novel design for an electrolyte with modified transport, in which anions were fixed in space to reduce the electric field at the lithium metal (Fig. 1A). The fraction of the anions being immobilized ($C_{a,f0}$) is treated as variable, such that the system collapses to the conventional solid electrolyte for $C_{a,f0} = 0$, whereas the opposite extreme of $C_{a,f0} = 1$ models a single-ion conductor. Such a system may be realized by either tethering anions to the walls of a porous medium, adopting polyelectrolyte separators, or using single-ion conductors as additives to a conventional salt electrolyte. The design was motivated by several studies (*1*, *2*, *24*–*26*), which showed that electrodeposition was destabilized by large electric fields near the lithium electrode, leading to preferential deposition on dendritic tips. Such electrolytes were shown to be effective in slowing the growth rate of instabilities in electrodeposition, which are responsible for dendritic growth (*27*). Here, we examine the combined effect of these physics and separator mechanics. A specific goal is to critically evaluate, by theoretical analysis, the possibility of reducing the value of the critical separator modulus proposed by Monroe and Newman (*12*) through tethered anion electrolytes/separators. Because tethering of anions modifies the transport across the separator, the results reported here reveal how the interplay of the two effects—elastic deformation of the separator and the electrode, and ion transport across the separator—sets the necessary criteria for stable electrodeposition and reduced dendritic growth rate. For this first study, we focus only on solid electrolytes and in so doing leave out convective effects. In liquids and viscoelastic media, significant bulk- and interface-driven electroconvection effects are expected, which may provide additional mechanisms by which instability is promoted or suppressed (*28*).

In studying the effects of separator elasticity and charge immobilization on the stability of electrodeposition, we will demonstrate a single framework that combines the roles of separator and electrode mechanics and the electrochemistry in deposition. Using this, we will first analyze the deformation and transport across a solid, nanostructured separator between two perfectly flat electrodes. We will then perform a linear stability analysis of the planar deposition by sinusoidally perturbing the metal electrode surface and determining the growth rate of the perturbation. One can describe any small-amplitude perturbation as a sum of sinusoids, and the initial growth of various Fourier modes is decoupled in the linear regime. The linear stability analysis thus provides a description of the growth of various Fourier modes of the electrode surface corrugations, which can then be used to determine the conditions necessary to suppress the growth of any given mode. Of particular interest is the dependence of growth rate on separator modulus, fraction of immobilized anions, and the applied current density. We will also determine whether it is possible to reduce the critical separator modulus required to suppress dendrite formation by changing the current density and fraction of immobilized anions, which are normally more readily varied than the separator modulus.

We consider the effect of elastic deformation on the transport of ions through the tethered anion separator. The elastic deformation problem is solved assuming linear, elastic, Hookean deformations of the separator and metal electrode. The counterelectrode is assumed to be rigid. The growth of the electrode and separator is dictated by transport of ions across their interface, and the electrode profile is obtained by imposing the constraint that the separator and electrode are to remain in contact with each other at all times. The elastic stresses also change the pressure in the separator, which in turn affects the concentrations of the ions through its contribution to their chemical potentials and therefore the equilibrium condition at the electrode surface. Thus, we have a coupled problem where transport affects the deformation of the separator and metal electrode, and the deformation of the separator drives the transport of ions through the separator.

We discuss the deformation and transport problems in the two subsequent subsections while noting the factors that lead to their coupling. These can then be solved together to obtain the solution for growth of the electrode profile with time.

The transport problem

In formulating our transport equations, we model our electrolytes as ideal solutions for simplicity. The local chemical potential of the lithium ion (ψ_c) and the mobile anion ($\psi_{a,m}$) in the separator can be written in terms of concentrations C_c and $C_{a,m}$, electrostatic potential ϕ, and pressure in the separator p^s

$$\psi_c = \psi_c^\theta + RT \ln C_c + F\phi + v_c p^s \quad (1)$$

$$\psi_{a,m} = \psi_{a,m}^\theta + RT \ln C_{a,m} - F\phi + v_{a,m} p^s \quad (2)$$

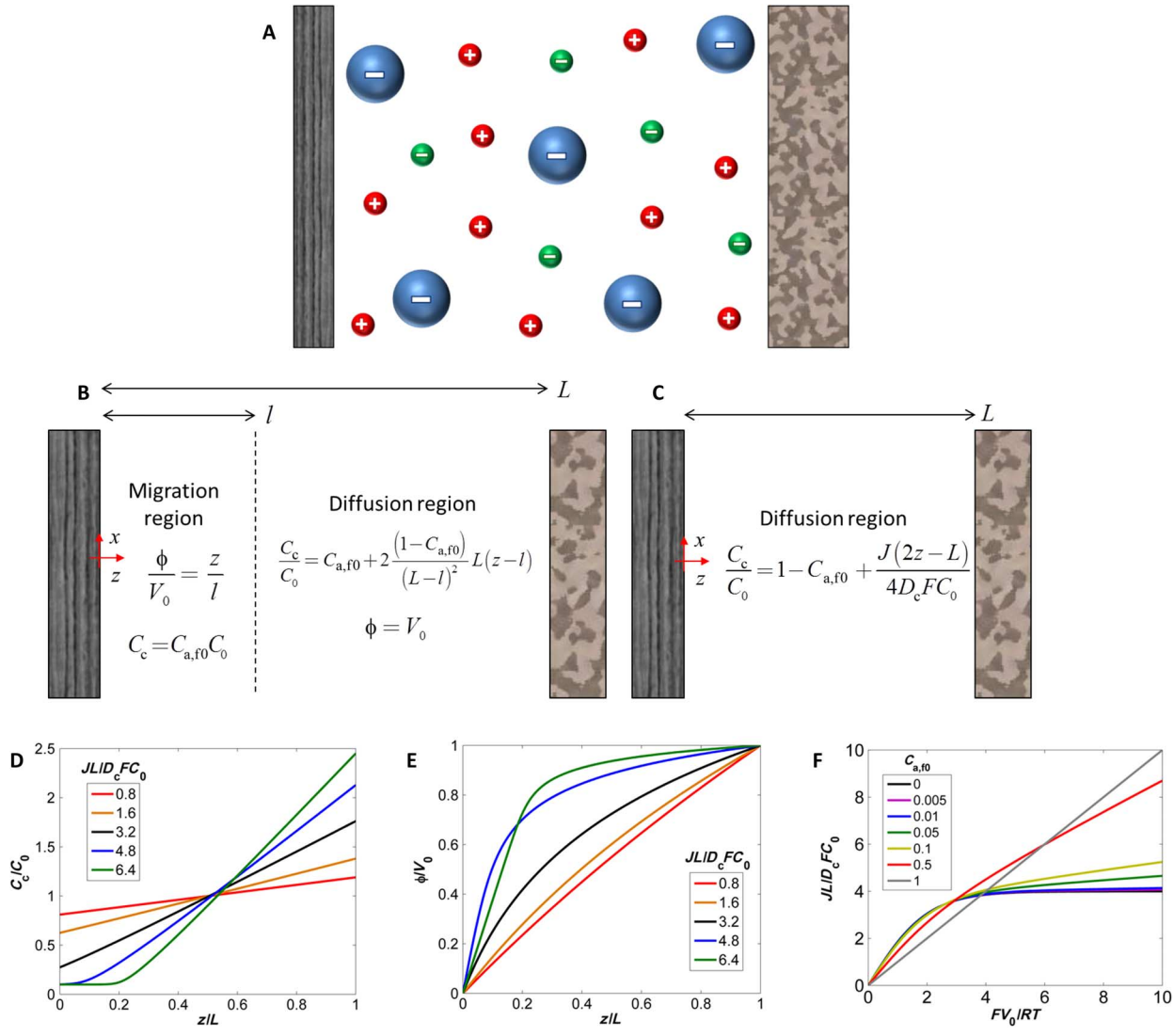

Fig. 1. Introduction to the electrolyte with immobilized anions. (**A**) An illustration of the electrolyte. The large blue spheres denote the anions immobilized by tethering to a solid matrix. The small green and red spheres indicate the mobile anions and cations. (**B** and **C**) An approximate solution to the base state problem at steady state for (B) high current densities and (C) low current densities, as shown in a previous work (*25*). Above the critical current density $J_{cr} = 4D_cFC_0(1 - 2C_{a,f0})/L$, the migration region that is devoid of mobile anions forms near the metal electrode. The same solution is valid even with the inclusion of pressure gradient–driven transport, because pressure in the separator is uniform in the base state. (**D** and **E**) Base state solution to the steady-state transport problem: (D) cation concentration and (E) electric potential. The fraction of immobilized anions $C_{a,f0}$ is 0.1, yielding a critical current density J_{cr} of $3.2D_cFC_0/L$. The profiles at the critical current density are indicated by the solid black lines. (**F**) Current density–voltage characteristics for various fractions of immobilized anions.

Here, v_c and $v_{a,m}$ are the partial molar volumes of the cation and the mobile anion in the separator. T represents temperature, and R and F are the ideal gas constant and Faraday's constant, respectively. The fluxes of each ion can be derived from the gradients of chemical potentials as

$$\mathbf{N}_c = -\mu_c C_c \nabla \psi_c = -RT\mu_c \nabla C_c - F\mu_c C_c \nabla \phi - v_c \mu_c C_c \nabla p^s \quad (3)$$

$$\mathbf{N}_{a,m} = -\mu_{a,m} C_{a,m} \nabla \psi_{a,m} = -RT\mu_{a,m} \nabla C_{a,m} + F\mu_{a,m} C_{a,m} \nabla \phi - v_{a,m} \mu_{a,m} C_{a,m} \nabla p^s \quad (4)$$

In each of the two equations above, the first term on the right-hand side represents diffusion of the respective ion, the second term describes the migration of the ion under the action of the externally applied electric field, and the third term refers to the motion of the ion under the local pressure gradient (*29*–*31*). The expressions include the Einstein relation between diffusivity and mobility for both the cation and mobile anion, that is, $D_c = RT\mu_c$ and $D_{a,m} = RT\mu_{a,m}$. We also assume that the mobile anion is in equilibrium and the current is carried entirely by the cation. Local electroneutrality is assumed, which gives $C_c = C_{a,m} + C_0C_{a,f}$.

The concentration of the fixed anions is also affected by the local deformation field, which compresses the matrix. Consider a

three-dimensional element of volume V in the stressless matrix of fixed anion concentration $C_{a,f0}$. After deformation, the volume of the element becomes $V + \delta V$, and the concentration of the fixed anions becomes $C_{a,f}$. By conservation of fixed charges within the element, we have $C_{a,f0}V = C_{a,f}(V + \delta V)$. Noting that $\delta V/V$ is the volumetric strain in the matrix and is related to the deformation field as $\delta V/V = \nabla \cdot \mathbf{u}^s$, we get

$$C_{a,f} = C_{a,f0}(1 - \nabla \cdot \mathbf{u}^s) \tag{5}$$

The above governing equations are subject to boundary conditions of chemical equilibrium of the cation and no flux of the mobile anion at the separator-counterelectrode and metal-separator interfaces. Chemical equilibrium at the metal-separator interface implies

$$\psi_c^\theta + RT \ln C_c + F\phi + \nu_c p^s = \psi_m^\theta + F\phi_m + \nu_m p^m \tag{6}$$

The equilibrium at the separator-counterelectrode interface is similar, but without the term with the pressure in the electrode. In doing this, we assume that the storage in the counterelectrode involves intercalation, which does not modify its chemical potential appreciably.

To evaluate the local pressure and deformation field, we, like Monroe and Newman (*12*), use the laws of linear elasticity. As will soon become apparent, the elasticity plays no role in the transport for flat, parallel electrodes. This is due to the fact that pressure in the separator is uniform in the case of planar electrodeposition. When performing the linear stability analysis with small sinusoidal perturbations, we will have small deformations of the electrode and the separator so that linear elasticity is applicable.

The deformation problem

For an isotropic separator with linear elasticity, we can write the stress tensor in terms of the local deformation field $\mathbf{u}^s$ as

$$\boldsymbol{\sigma}^s = \frac{2\nu^s G^s}{1 - 2\nu^s}(\nabla \cdot \mathbf{u}^s)\mathbf{I} + G^s\left[\nabla \mathbf{u}^s + (\nabla \mathbf{u}^s)^\dagger\right] \tag{7}$$

where G^s and ν^s are the shear modulus and the Poisson ratio of the separator. "†" denotes the transpose operation, and $\mathbf{I}$ is the identity tensor. The pressure is given by the trace of the stress tensor as

$$p^s = -\frac{1}{3}tr(\boldsymbol{\sigma}^s) = -K^s \nabla \cdot \mathbf{u}^s \tag{8}$$

K^s is the bulk modulus of the separator and is related to G^s and ν^s as $K^s/G^s = 2/3\ (1 + \nu^s)/(1 - 2\nu^s)$. The local force balance on the separator implies $\nabla \cdot \boldsymbol{\sigma}^s = 0$. This gives

$$\nabla^2 \mathbf{u}^s + 2\alpha^s \nabla(\nabla \cdot \mathbf{u}^s) = 0 \tag{9}$$

A similar balance for the metal and the pressure in the metal is obtained as

$$\nabla^2 \mathbf{u}^m + 2\alpha^m \nabla(\nabla \cdot \mathbf{u}^m) = 0 \tag{10}$$

$$p^m = -K^m \nabla \cdot \mathbf{u}^m \tag{11}$$

Here $\alpha^s = 1/[2(1 - 2\nu^s)]$ and $\alpha^m = 1/[2(1 - 2\nu^m)]$ are related to the Poisson ratios of the separator and metal. The counterelectrode is assumed to be rigid.

The boundary conditions to the deformation problem are given by force balance and continuity of deformation at the separator-metal and separator-counterelectrode interfaces. At the separator-metal interface, we consider surface tension of the interface to act as a normal force on the metal electrode. The force balance can then be written as

$$\mathbf{e}_n \cdot \boldsymbol{\sigma}^s|_{Hc} = \mathbf{e}_n \cdot \boldsymbol{\sigma}^m|_{Hc} + \gamma K \mathbf{e}_n \tag{12}$$

Here, $\mathbf{e}_n$ is the unit normal to the surface of the electrode into the separator, γ is the surface tension, and K is the local electrode curvature. For small deformations of the electrode surface profile H_c in the x direction, the curvature is given by $K = d^2H_c/dx^2$.

The continuity of tangential deformation is written similarly as

$$(\mathbf{I} - \mathbf{e}_n\mathbf{e}_n) \cdot \mathbf{u}^m|_{Hc} = (\mathbf{I} - \mathbf{e}_n\mathbf{e}_n) \cdot \mathbf{u}^s|_{Hc} \tag{13}$$

The normal deformation of the metal electrode and separator is given by the difference between the final electrode profile and its stress-free state. The stress-free state of the electrode is modified by transport and grows because of the cations getting assimilated on the electrode surface. Likewise, the separator surface is also determined by the transport of cations across the metal-separator interface. This interpretation assumes that the growth of the unstressed electrode and separator due to transport remains stressless. The stress in the deformed electrode and separator and their surface profiles comes from the constraint that the electrode and separator are required to remain in contact with each other at all times.

Hence, the stress-free profiles of the electrode (H_{sf}^m) and separator (H_{sf}^s) surfaces are given as

$$\frac{\partial H_{sf}^m}{\partial t} = -\nu_m \frac{(\mathbf{e}_n \cdot \mathbf{J})|_{H_c}}{F} \tag{14}$$

$$\frac{\partial H_{sf}^s}{\partial t} = -\nu_c \frac{(\mathbf{e}_n \cdot \mathbf{J})|_{H_c}}{F} \tag{15}$$

Here, $\mathbf{J}$ is the current density vector of magnitude J, and ν_m is the partial molar volume of the metal in the electrode. The current density vector is obtained from Faraday's laws of electrolysis as $\mathbf{J} = F(\mathbf{N}_c - \mathbf{N}_{a,m})$. The deformation of the separator and electrode at the surface is given by

$$\mathbf{e}_n \cdot \mathbf{u}^m|_{Hc} = H_c - H_{sf}^m \tag{16}$$

$$\mathbf{e}_n \cdot \mathbf{u}^s|_{Hc} = H_c - H_{sf}^s \tag{17}$$

This boundary condition is different from the corresponding one used by Monroe and Newman (*12*). They regard the normal deformation as the imposed perturbation, which may be obtained by eliminating H_{sf}^m and H_{sf}^s from Eqs. 16 and 17, respectively. This will

be the case if the interface is deformed by an external force and will, hence, yield an unusually conservative estimate of the separator modulus required to suppress the instabilities. The present formulation incorporates transport-driven growth of the electrode profile, thus expressing the stability as a net result of the competing factors of transport-driven destabilization and elasticity-promoted stabilization.

RESULTS

We start by solving the electrodeposition problem for planar, parallel, semi-infinite electrodes, with all deformations and fluxes in the z direction, normal to the electrodes. In this case, we find that the pressure gradient terms in the transport equations vanish, because pressure in the separator is uniform. The transport is governed by diffusion-migration of the cation and mobile anion with fast reaction kinetics at the two interfaces. We have previously shown that the solution for transport for such a case exhibits two qualitatively different behaviors (Fig. 1, B and C). At small current densities, the transport is governed primarily by ambipolar diffusion of the cation throughout the separator (Fig. 1C). Above a critical current density given as $J_{cr} = 4D_cFC_0(1 - 2C_{a,f0})/L$, the mobile anions are depleted at the metal electrode, leading to the formation of a depletion zone, where the cation exists solely to neutralize the fixed anions (*32*). The mobile anions accumulate against the counterelectrode, causing the interelectrode region to be divided into two zones: the diffusion region having ambipolar diffusion of the cation, and the migration region that is depleted of the mobile anion and where the primary transport mechanism is the electric field–driven migration of the cations neutralizing the mobile anions (Fig. 1B). The plots for the exact base state solutions for the cation concentration and electric potential profiles are shown in Fig. 1 (D and E) (*27*). Figure 1F shows the current density–voltage characteristics for various values of the fixed anion fraction. The current-voltage response contains two constant slope regions: one below the critical current density and one above it. The size of the low–current density regime is observed to decrease with the fraction of fixed anions. Thus, in systems where the fraction of immobilized charge is not known a priori, the current-voltage characteristics for the electrolyte may be used to estimate it.

Next, we perform a linear stability analysis of the base state transport solution by introducing regular perturbations to the electrode surface ($\tilde{H}_c = H_c + \varepsilon e^{\sigma t} e^{ikx}$) of arbitrarily small amplitude ε and known wave number k. For small amplitudes, the perturbations to the concentration [$\tilde{C}_c = C_c + \varepsilon C_c'(z) e^{\sigma t} e^{ikx}$], potential [$\tilde{\phi} = \phi + \varepsilon \phi'(z) e^{\sigma t} e^{ikx}$], and current density [$\tilde{\mathbf{J}} = \mathbf{J} + \varepsilon \mathbf{J}'(z) e^{\sigma t} e^{ikx}$] are also expected to vary in the same manner. The deformation fields in the separator [$\tilde{\mathbf{u}}^s = \mathbf{u}^s + \varepsilon \mathbf{u}^{s'}(z) e^{\sigma t} e^{ikx}$] and the electrode [$\tilde{\mathbf{u}}^m = \mathbf{u}^m + \varepsilon \mathbf{u}^{m'}(z) e^{\sigma t} e^{ikx}$] are also perturbed in a regular fashion. The amplitudes of the perturbations grow with time if the real part of σ is positive, which implies unsteady electrodeposition leading to dendritic structures.

Linear stability at large current densities

The two-region model for high current densities is linearly perturbed, as mentioned above and illustrated in Fig. 2 (A and B) (also see Materials and Methods). This includes a perturbation to the boundary l between the diffusion and migration regions. The governing equations for transport are given by Stokes equations for cation concentration and potential in the diffusion and migration regions, respectively. It is important to note that the pressure gradient term is no longer absent because the perturbation gives nonuniform pressure within the separator. See the Supplementary Materials for full equations.

The perturbed equations can be solved in the large kL limit analytically. This limit is appropriate for describing LMB experiments, for which the widths of morphological instabilities (~1 μm) are much smaller than the typical interelectrode distance (~1 mm). The following results are for values of $kL > 5$, which corresponds to dendrite widths of less than 628 μm. Under such conditions, the counterelectrode is so far away that the perturbations to cation concentration and separator deformation field decay to insignificant values before they reach it. The perturbation growth rate is obtained as

$$\sigma = \frac{\nu_m}{(1 - c_3^m)F}\left[kJ - \nu_m \mu_c K^m F C_{a,f0} C_0 k Z_1^m - \frac{1}{2}\left(1 - e^{-2kl}\right) J Z_1^s + \frac{K^s(\nu_c + \nu_{a,m})}{4RT} J Z_1^s e^{-2kl}\right] \quad (18)$$

where Z_1^m, c_3^m, and Z_1^s are obtained from the solutions of

$$Z_1^m\left[\frac{1 + 2\alpha^m}{1 + 2\alpha^s} G + \frac{1 + \alpha^m}{1 + \alpha^s}\right] - c_3^m k\left[\frac{2(G - V)}{1 + 2\alpha^s} + \frac{1 + V}{1 + \alpha^s}\right] = -k\frac{1 - V}{(1 + \alpha^s)(1 + 2\alpha^s)} \quad (19)$$

$$Z_1^m[1 + \alpha^m + \alpha^m G] - c_3^m k[1 - V] = -\frac{1}{2}\frac{\gamma}{G^s}k^2 - k[1 - V] \quad (20)$$

$$Z_1^s[1 + \alpha^s] = Z_1^m[1 + \alpha^m] - c_3^m k[1 + V] - k[1 - V] \quad (21)$$

with G and V related to the moduli and partial molar volume of the cation in the two phases, namely, separator and electrode, as

$$G = \frac{G^m}{G^s} \quad (22)$$

$$V = \frac{\nu_c}{\nu_m} \quad (23)$$

Thus, to obtain the growth rate of the perturbations, we first solve a set of linear algebraic equations (Eqs. 19 to 23) for Z_1^m, c_3^m, and Z_1^s and then calculate σ from Eq. 18.

The result in Eq. 18 is unaffected by the boundary conditions at the counterelectrode because we have assumed $kL >> 1$ so that the perturbations decay before they reach the counterelectrode. The net result is therefore solely dependent on the conditions in the neighborhood of the metal electrode. Each term in Eq. 18 represents a particular mechanism influencing the perturbation growth rate, as summarized in Table 1. The first term of the expression in the square brackets refers to the convergence of electrical flux on the tips of the perturbation caused by interfacial deformation alone. This is the primary mechanism for the roughening of the interface. This term varies linearly with the deposition rate and is hence proportional to the current density.

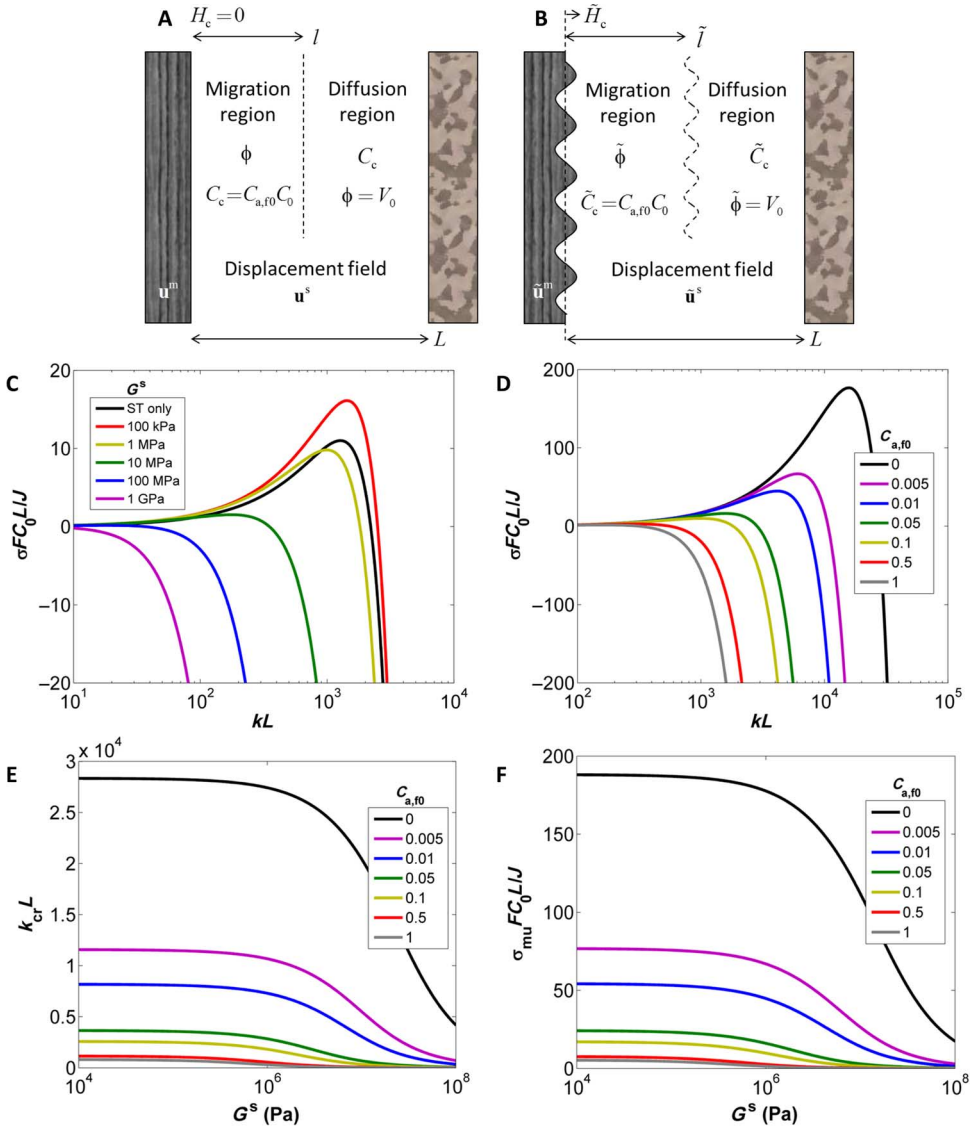

Fig. 2. Linear stability at large current densities. (**A** and **B**) Base state (A) and perturbed state (B) of the problem. (**C** and **D**) Growth rate versus wave number plots for (C) $C_{a,f0}$ = 0.1 with varying G^s, and (D) G^s = 1 MPa with varying $C_{a,f0}$. The black line in (C) corresponds to the result with elasticity excluded and only the effect of surface tension being considered. (**E** and **F**) Critical wave number (E) and growth rate (F) of the most unstable mode as a function of separator shear modulus for various fractions of immobilized anions.

Table 1. Transport mechanisms and their stabilizing behavior based on parameter values used in the paper.

Term number	Term in Eq. 18	Transport mechanism		Destabilizing/stabilizing
1	kJ	Electric flux due to surface deformation		Destabilizing
2	$\nu_m \mu_c K^m F C_{a,f0} C_0 k Z_1^m$	Change of reaction equilibrium due to electrode pressure caused by:	(i) Separator modulus	Stabilizing
			(ii) Surface tension	Stabilizing
3	$\frac{1}{2}\left(1 - e^{-2kl}\right) J Z_1^s$	Change in ionic conductivity in migration region due to separator compression		Destabilizing
4	$\frac{K^s(\nu_c+\nu_{a,m})}{4RT} J Z_1^s e^{-2kl}$	Pressure-driven flux in diffusion region. Pressure caused by:	(i) Separator modulus	Stabilizing
			(ii) Surface tension	Destabilizing

The second term represents the effect of stresses on the equilibrium at the electrode-separator interface. Regions of higher pressure in the electrode experience elasticity-induced reaction retardation because of the larger pressure work needed to reduce a cation and form a metal atom at the interface. For separators with small moduli, surface tension of the metal-separator interface serves the role of modulating the electrode pressure and thereby altering the reaction equilibrium. The third term reflects the effect of spatial variations in electrolyte conductivity near the electrode surface caused by separator deformation. As seen before, compression of the separator matrix increases the local concentration of the tethered anions. In a separator with a spatially varying deformation field, this matrix compression causes a spatial variation in the concentration of the tethered anions and, through electroneutrality, the local cation concentration and ionic conductivity. This also affects the current distribution to the electrode surface, because regions of higher conductivity experience higher current densities and faster deposition. Finally, the last term reflects the influence of the diffusion region on the stability of deposition. Whereas high pressure tends to increase the concentration of the immobilized salt by compression of the solid matrix to which the salt is tethered, the mobile salt is driven by the pressure-driven flux from high- to low-pressure locales in the separator because of the chemical potential gradient mentioned earlier in Eqs. 3 and 4. For perturbation wavelengths comparable to or smaller than the migration region thickness, the diffusion region has a significant contribution to the growth of such perturbations. This phenomenon will predictably supplant the matrix compression effect at small current densities, where the migration region is absent.

To evaluate the growth rate of the perturbations per mole of metal electrodeposited, we scale the growth rate with current density to account for the inherent increase in growth rate with current density. The wave number is multiplied by the separator thickness, which is the primary length scale for transport in the base state. Because the wave number provides the length scale for transport in the perturbed state, this scaling benchmarks the perturbed state against the base state. The scaled growth rate is plotted in Fig. 2 (C and D). The values of parameters used in these plots are as follows: $\nu_c = -8 \times 10^{-6}$ m^3/mol, $\nu_{a,m} = 1.78 \times 10^{-4}$ m^3/mol (*33*), $\nu_m = 1.3 \times 10^{-5}$ m^3/mol, $\nu^m = \nu^s = 0.33$, $G^m = 3.4$ GPa, $\gamma = 1.716$ N/m (*12*), $L = 1$ mm, which are specific to the electrodeposition of lithium. The values for ν_c and $\nu_{a,m}$ are specifically for lithium (Li^+) and bis(trifluoromethane) sulfonimide [$TFSI^-$ or $(CF_3SO_2)_2N^-$] ions in ethylene glycol (*33*) and will obviously change with the electrodeposition system. We here use the value reported by Marcus and Hefter (*33*) from rigorous experiments with various salts with a reference of a large ion's van der Waals volume, when no solvation effects are expected.

For the chosen parameter values, we find that the contributions of the first and third terms in Eq. 18 to σ are positive, whereas those of the second and last terms are negative. The growth of the perturbation by concentration of electric flux lines is destabilizing, as expected. The compressive stress in the electrode is stabilizing because the pressure in the electrode is higher at the peaks, thus creating an elasticity-induced retardation of the deposition on the peaks. The effect of separator matrix compression on the local ionic conductivity is destabilizing. This is also reasonable; the separator is compressed on perturbation peaks and dilated in the valleys, giving a higher fixed anion concentration on the peaks. Consequently, the conductivity is higher on the peaks, increasing the cation flux on the peaks in addition to the flux concentration mechanism of the first term. The last term, which describes the pressure-driven flux in the diffusion region, is stabilizing because the higher pressure in the peaks drives the ions into the low pressure valleys. This term is important for large wavelength perturbations (small k), but its significance diminishes quickly at higher k. The last two terms are absent if the analysis is performed without including the elastic deformation (*27*).

Figure 2C shows the variation of the scaled growth rate with wave number for a fixed anion fraction of 0.1, for various values of separator shear modulus, whereas Fig. 2D depicts the same variation for varying fixed anion fractions at a constant separator modulus of 1 MPa. Both figures suggest that small wave number perturbations are unstable, whereas the large wave number perturbations are rendered stable by the combined effect of the elasticity-induced reaction retardation and surface tension. The stability of electrodeposition is improved by increasing both the fraction of immobilized anions and the separator shear modulus. The small difference between the low modulus (100 kPa) case and the result obtained previously in an analysis that ignored elastic deformation (*27*) originates from the second term in Eq. 18, which describes the effect of separator matrix compression on the local ionic conductivity. Although this mechanism makes the growth rate in a low modulus electrolyte different from that in a hypothetical case that ignores both elastic stresses and deformation, the difference is modest, meaning that for LMBs based on low modulus polymer or gel polymer electrolytes, the previous analysis provides a sufficiently accurate result to guide material design.

The wave number dependence in Fig. 2 (C and D) can be analyzed further by extracting the wave number of the marginally stable mode, also called the critical wave number k_{cr}, and the growth rate of the least stable mode σ_{mu}. The critical wave number is the value of k at which σ changes sign from positive to negative. It corresponds to the physical situation where the driving forces for destabilizing the deposition, namely, transport, are equal to the stabilizing driving forces of surface tension and elasticity. This mode is thus neutrally stable and would correspond to the smallest observable sizes of the morphological instabilities. The most unstable mode corresponds to the value of k at which the largest growth rate is predicted. If the initial growth rate is indicative of the surface perturbations that continue to grow fastest at finite amplitude, then this will be the most prominently observed length scale of the surface roughness or dendrite size on the metal surface.

It is apparent from Fig. 2 (E and F) that both parameters can be reduced by increasing the fraction of fixed anions and the separator/electrolyte modulus, leading to improved stability of deposition. It is also important to note that the improvement in the stability of deposition is achieved at lower separator moduli by immobilizing a fraction of anions. This effect is dramatic within the first 10% of tethering and more gradual thereafter, meaning that one need not use single-ion conductors to observe them in laboratory experiments.

Linear stability at small current densities

Below the critical current density, transport across the separator is driven by ambipolar diffusion and pressure gradient–driven flux. On perturbing it, therefore, as shown in Fig. 3 (A and B) and solving the resultant set of equations in the large k limit gives

$$\sigma = \frac{\nu_m}{(1-c_3^m)F}\left[kJ - \nu_m \mu_c K^m F C_c|_0 k Z_1^m + \frac{K^s(\nu_c+\nu_{a,m})}{4RT} J Z_1^s\right] \quad (24)$$

where Z_1^m, c_3^m, and Z_1^s are obtained from Eqs. 19 to 23.

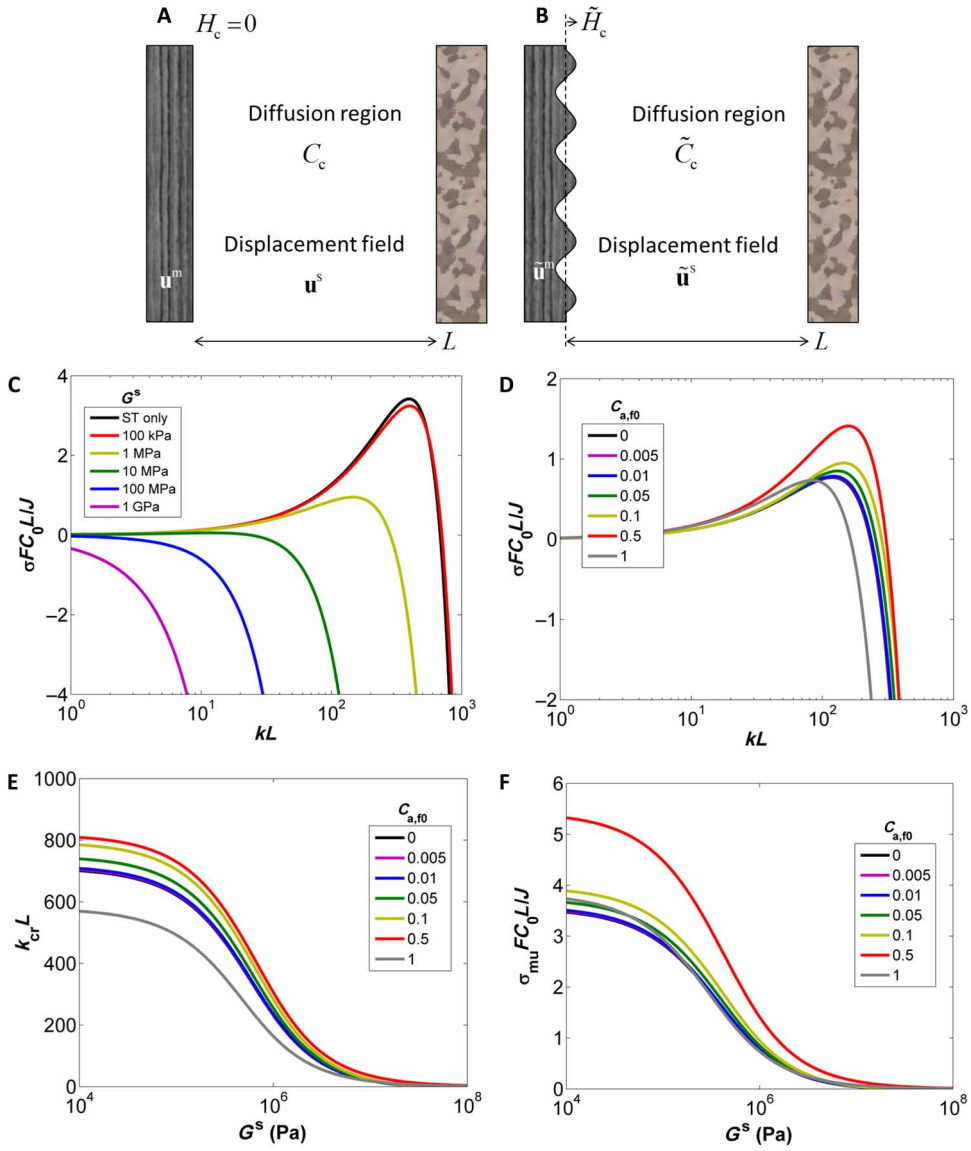

Fig. 3. Linear stability at small current densities. (**A** and **B**) Base state (A) and perturbed state (B) of the problem. (**C** and **D**) Growth rate versus wave number plots for (C) $C_{a,f0}$ = 0.1 with varying G^s, and (D) G^s = 1 MPa with varying $C_{a,f0}$. The black line in (C) corresponds to the result with elasticity excluded and only the effect of surface tension being considered. (**E** and **F**) Critical wave number (E) and growth rate (F) of the most unstable mode as a function of separator shear modulus for various fractions of immobilized anions.

Comparing each of the terms in square brackets in Eq. 24 to their corresponding counterparts in Eq. 18, we find that the first two terms represent the convergence of electrical flux and electrode compression, respectively, whereas the last term in Eq. 24 is like the last term in Eq. 18, namely, the contribution of pressure gradient–driven transport. As with the case of high current densities, the convergence of flux on perturbation tips is destabilizing, whereas compression of the electrode and the pressure-driven flux are stabilizing. The third term in Eq. 18 representing the matrix compression effect is absent here because the current densities are lower than the critical value required for forming the migration region.

The plots for current density normalized growth rate for small current densities are shown in Fig. 3 (C and D). The critical wave number and the growth rate of the least stable mode are plotted in Fig. 3 (E and F). The effect of anion tethering is less pronounced in this case because the current is primarily carried by the mobile salt. The growth rates are also smaller because of the smaller current densities. The role of separator elasticity is the same as in the high current densities case.

The large and small current density results are compiled in fig. S1, which shows the variation of the critical wave number with current density for various fixed anion fraction and separator modulus. As expected, the critical wave number increases with current density, reflecting the decreased stability of deposition because of higher flux concentrating on the perturbation tips. This is consistent with the observations of several studies that dendrite proliferation was promoted at higher current densities (*20*–*23*). The effectiveness of the anion

tethering (fig. S1A), which was demonstrated in recent studies (*34*–*36*), and the suppression effect of higher separator moduli (fig. S1B) noted by Stone *et al.* (*13*) are also seen in the reduction of the critical wave number of the perturbation. It is also important to note that stability of all modes can be achieved, as can be seen in the cases of G^s = 1 GPa in Fig. 2B and G^s = 100 MPa and 1 GPa in Fig. 3C.

Dimensional analysis

In the presentation above, we have shown the stability characteristics for dimensional parameters chosen to reflect lithium ion transport to a lithium metal electrode through ethylene glycol. We noted that the stability results from four mechanisms: the destabilizing effect of convergence of electrical flux on perturbation tips, the stabilizing roles of pressure-driven flux from high- to low-pressure regions, elasticity-induced reaction retardation of the deposition process, and surface tension of the metal-separator interface. Although this is an important application of current interest for high–energy density LMB electrolyte and separator design, it is also valuable to consider the present analysis in a broader context. For this purpose, we introduce the dimensionless parameters that govern the problem. We choose L as the length scale for all spatial parameters in the interelectrode space because it is the characteristic length for transport in the base state problem. Deformation fields in the electrolyte are also scaled by L. Deformation fields in the metal are scaled by LG^s/G^m to account for the difference in moduli of the separator and metal. All concentrations are scaled by the equilibrium salt concentration C_0, and chemical potentials are scaled by RT. Pressure and stresses in the separator are scaled by the separator modulus G^s, whereas the electrode stresses and pressure are nondimensionalized by the electrode modulus G^m. The growth rate is scaled as J/FC_0L to account for its inherent increase with increasing current density, as mentioned earlier. The above equations are thus nondimensionalized as $x^* = x/L$, $z^* = z/L$, $\tilde{l}^* = \tilde{l}/L$, $\tilde{\mathbf{u}}^{s*} = \tilde{\mathbf{u}}^s/L$, $\tilde{\mathbf{u}}^{m*} = \tilde{\mathbf{u}}^m G^m/LG^s$, $k^* = kL$, $\sigma^* = \sigma FC_0L/J$, $\tilde{C}_c^* = \tilde{C}_c/C_0$, $\nu_c^* = \nu_c C_0$, $\nu_{a,m}^* = \nu_{a,m} C_0$, $\nu_m^* = \nu_m C_0$, $\tilde{p}^{s*} = \tilde{p}^s/G^s$, $\tilde{p}^{m*} = \tilde{p}^m/G^m$, $K^{s*} = K^s/G^s$, $K^{m*} = K^m/G^m$, $J^* = JL/D_cFC_0$. Some parameters such as the Poisson ratios ν^s and ν^m, α^s and α^m, and the ratios of metal to separator modulus, G, and partial lithium partial molar volume, V, are dimensionless and are retained as such. The critical current density for the transition from small current densities to large current densities then becomes $J_{cr}^* = 4(1 - 2C_{a,f0})$.

The nondimensional form for the growth rate at high current densities expressed in Eq. 18 is then obtained as

$$\sigma^* = \frac{\nu_m^*}{1 - c_3^{m*}}\left[k^* - \frac{1}{\mathrm{Ee}} K^{m*} C_{a,f0} k^* Z_1^{m*} - \frac{1}{2}\left(1 - e^{-2k^*l^*}\right) Z_1^{s*} + \frac{1}{4} K^{s*}\,\mathrm{Eo} Z_1^{s*} e^{-2k^*l^*}\right] \quad (25)$$

where Z_1^{m*}, c_3^{m*}, and Z_1^{s*} are obtained from the nondimensional forms of Eqs. 19 to 23

$$\frac{Z_1^{m*}}{G}\left[\frac{1 + 2\alpha^m}{1 + 2\alpha^s} G + \frac{1 + \alpha^m}{1 + \alpha^s}\right] - \frac{c_3^{m*}}{G} k^* \left[\frac{2(G - V)}{1 + 2\alpha^s} + \frac{1 + V}{1 + \alpha^s}\right] = -k^* \frac{1 - V}{(1 + \alpha^s)(1 + 2\alpha^s)} \quad (26)$$

$$\frac{Z_1^{m*}}{G}[1 + \alpha^m + \alpha^m G] - \frac{c_3^{m*}}{G} k^*[1 - V] = -\frac{1}{2}\,\mathrm{Ec} k^{*2} - k^*[1 - V] \quad (27)$$

$$Z_1^{s*}[1 + \alpha^s] = \frac{Z_1^{m*}}{G}[1 + \alpha^m] - \frac{c_3^{m*}}{G} k^*[1 + V] - k^*[1 - V] \quad (28)$$

Similarly, for the small current densities case, we obtain

$$\sigma^* = \frac{\nu_m^*}{1 - c_3^{m*}}\left[k^* - \frac{1}{\mathrm{Ee}} K^{m*} C_c^*|_0 k^* Z_1^{m*} + \frac{1}{4} K^{s*}\,\mathrm{Eo} Z_1^{s*}\right] \quad (29)$$

where Z_1^{m*}, c_3^{m*}, and Z_1^{s*} are obtained from Eqs. 26 to 28.

Three nondimensional numbers appear in the above analysis. The first dimensionless group is seen in the second term of the parentheses in Eqs. 25 and 29. We define it as the electrical-elastic number Ee

$$\mathrm{Ee} = \frac{JL}{\nu_m \mu_c FC_0 G^s} \quad (30)$$

Ee compares the relative importance of convergence of electrical flux on perturbation tips and elasticity-induced retardation of the deposition reaction on the tips. A smaller value of Ee favors stable deposition and can be attained by either reducing the current density or improving the separator modulus, cationic mobility, or salt concentration.

The second dimensionless group is the elasto-osmotic number as seen in the last terms in Eqs. 25 and 29, defined as the ratio of the shear elastic modulus to the osmotic pressure of the ions, and is expressed as

$$\mathrm{Eo} = \frac{G^s(\nu_c + \nu_{a,m})}{RT} \quad (31)$$

It reflects the ability of elastic stresses to alter the ion transport mechanisms by producing a pressure-driven flux in the diffusion region. As seen before, the convergence of electric flux on dendrite tips destabilizes deposition and causes perturbation growth. However, the elastic stresses in the separator caused by the perturbation growth create a pressure gradient that drives ions away from the perturbation tips, which we call the pressure-driven flux. It is important to consider this stabilizing mechanism, though secondary, because it has a significant role in determining the criterion of marginal stability, where the deposition is stable across all modes, which is addressed in the next section. The elasto-osmotic number compares the strength of the stabilizing effect of pressure-driven flux to the primary electric flux–driven destabilization. The elasto-osmotic number therefore reflects the separator elasticity nondimensionalized by transport in the diffusion region. A higher Eo value would favor stable deposition and may be achieved by increasing the separator modulus and the ionic partial molar volumes, both of which enhance the strength of the pressure-driven flux relative to the electric flux.

The third dimensionless group that appears in Eq. 27 is the elastocapillary number

$$\mathrm{Ec} = \frac{\gamma}{G^s L} \quad (32)$$

This group measures the relative effects of surface tension and elastic stresses and indicates whether surface tension or separator elasticity

has a more pronounced effect on the pressures in the electrode and the separator, which modulate the reaction equilibrium. Because both the surface tension and separator elasticity have stabilizing effects on the deposition, the elastocapillary number does not reflect on the stability of deposition. The role of surface tension becomes more important when $k^* > 1/\mathrm{Ec}$, as can be seen from Eq. 27, which happens at very small separator moduli or when the interfacial tension is large. The elastocapillary number also appears in descriptions of extensional deformations of polymers with free surfaces (*37*), contact of soft elastic solids with liquids (*38*), or other solids (*39*).

Although the three dimensionless groups defined above are sufficient to describe the growth rate, we can also define an electrical-Bond number Eb. This dimensionless group arises when Eq. 27 is substituted into Eqs. 25 and 29, from the combination of the electrical-elastic number Ee and the elastocapillary number Ec. As stated earlier, surface tension becomes important for deposition of modes where $k^* = O(1/\mathrm{Ec})$. This suggests that for extremely soft separators, the electrical-elastic number should be replaced by a different group, based on the convergence of electrical flux and surface tension. The number obtained is the electrical-Bond number Eb defined as

$$\mathrm{Eb} = \frac{\mathrm{Ee}}{\mathrm{Ec}} = \frac{JL^2}{\nu_m \mu_c F C_0 \gamma} \tag{33}$$

The electrical-Bond number (Eb) is the electrical analog of the better-known Bond number (*40*, *41*), which compares the role of gravitational forces to surface tension. In the present analysis, Eb compares the relative strength of electrical forces, here in the form of current density, to the surface tension. The electrical-elasticity number (Ee) can be thought of as the elasticity equivalent of the electrical-Bond number. Like Ee, a low electrical-Bond number would favor stable deposition, which suggests that reducing the current density or improving the surface tension, cationic mobility, or salt concentration would have a stabilizing impact.

The influence of these nondimensional groups on the stability at various separator moduli and deposition length scales is represented in the form of a map in Fig. 4. The elastic deformation of the separator plays two fundamental roles in improving the stability. First, it alters the chemical potential gradient of the ions through the pressure, as reflected in the second and fourth terms in the square parenthesis in Eq. 25 and the second term in Eq. 29. For the mobile salt, the pressure gradient in the electrolyte/separator generates a chemical potential gradient that drives the mobile salt away from regions of high pressure, which in the present case is on the perturbation tips. For separators less stiff than the metal electrode (that is $G^s << G^m$), the contribution made by the pressure gradient term, relative to the convergence of electrical flux on the perturbation tips, in stabilizing deposition can be written as Eo $(1 - V)$. The immobile salt, on the other hand, has a higher concentration in regions of high pressure, thus increasing the flux. For $G^s << G^m$, this term makes a contribution relative to the convergence of electrical flux as $1 - V$. The absence of a dependence on the elasto-osmotic number can be explained from the fact that this mechanism is based on the volumetric compression of the separator caused by the pressure rather than the actual value of the pressure itself. At small current densities where the transport is dominated by the mobile salt, this transport mechanism can stabilize the deposition for all modes for large separator moduli (region IV in Fig. 4A). For large current densities, the thickness of migration region controls the relative strengths of the mobile salt and the immobile salt in the stability of deposition. Therefore, the location of this boundary changes.

The second role played by elasticity in the stability analysis is through its effect on the interfacial dynamics, by retarding the deposition reaction on the perturbation tips. This phenomenon is captured in the third terms of Eqs. 25 and 29 for large and small current densities, respectively. The relative strength of this mechanism can be compared to the convergence of electrical flux on perturbation tips through the electrical-elastic number Ee and is wave number–dependent as k^*/Ee. The retardation of the deposition reaction thus outweighs the convergence of electrical flux for $k^* >> \mathrm{Ee}$ (region III in Fig. 4A). Reducing the separator modulus to extremely low values increases the electrical-elastic number, and thus, the elasticity-induced slowing of interfacial deposition becomes important only at larger k^*.

For even smaller separator moduli, surface tension is important relative to the separator elasticity and suppresses perturbation growth by electrical flux for $k^* \gg \sqrt{\mathrm{Eb}}$ (region II in Fig. 4). This is consistent with our previous result (*27*). The boundary between regions I and II indicates this transition. Similarly, the boundary between regions I and III denotes the transition from unstable deposition because of convergence of electrical flux and stable deposition caused

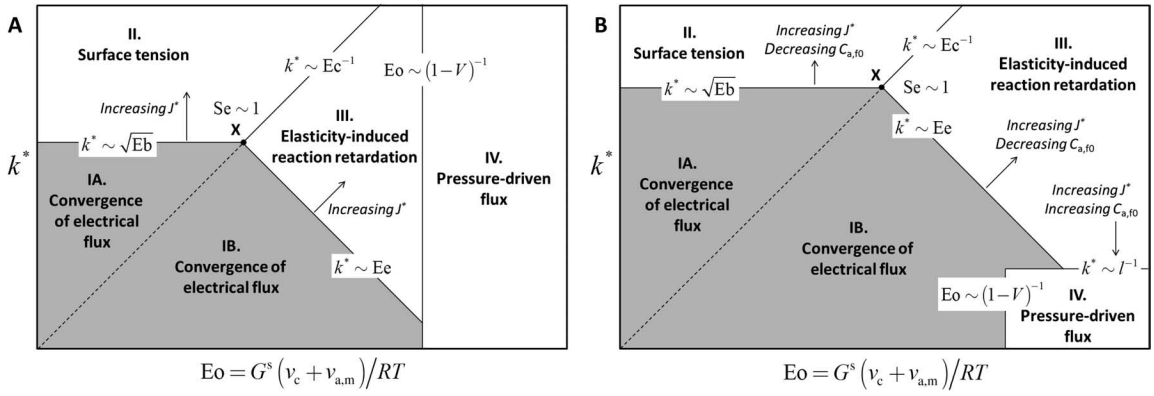

Fig. 4. State diagram of the dominant mechanism in stability. (**A** and **B**) Dominant mechanism in the stability of electrodeposition at various dimensionless wave numbers and separator moduli for (A) small current densities and (B) large current densities. The shaded region is unstable. See text for definitions of the various dimensionless groups.

by elasticity-induced reaction retardation, as seen earlier. The intersection of these two boundaries thus gives the transition from surface tension–induced stability to elasticity-caused stability, which can be predicted by a surface tension–elasticity number Se

$$\mathrm{Se} = \frac{\mathrm{Ee}}{\sqrt{\mathrm{Eb}}} = \frac{1}{G^{\mathrm{s}}}\sqrt{\frac{J\gamma}{\mu_{\mathrm{c}} F C_0 \nu_{\mathrm{m}}}} \tag{34}$$

For Se < 1, elasticity is the prominent mechanism for stability. For $J^* = 2$ and parameter values mentioned earlier, this transition happens for $G^{\mathrm{s}} > 0.81$ MPa.

Both the electrical-Bond (Eb) and electrical-elastic (Ee) numbers increase with current density. The boundaries between regions I and II, and regions I and III in Fig. 4A are hence dependent on current density, and region I, namely, the zone of converging electrical flux, expands as the square root of current density. The boundaries between regions II and III, based on the elastocapillary number (Ec) signifying the importance of surface tension relative to elasticity, remain invariant with current density. Region IV, which represents the role of pressure gradient–driven transport, is based on the elasto-osmotic number (Eo) and also remain independent of current density. Below the critical current density, the fixed anions have no contribution to transport, and hence, the above behaviors are independent of $C_{\mathrm{a,f0}}$.

Above the critical current density, the behaviors of Eb and Ee with current density remain the same as above, as can be seen in Fig. 4B. The formation of the migration region restricts the pressure gradient–driven transport to the now smaller diffusion region, thus shrinking region IV to modes smaller than the migration region thickness only, that is, $k^* < l^{-1}$. The migration region becomes thicker with increasing current density or fixed anion fraction, thus making this restriction stronger. The sizes of the other zones are also affected by $C_{\mathrm{a,f0}}$ at higher current densities because the immobile anions have a significant effect on cation transport. Increasing the fraction of fixed anions reduces the electric field at the metal electrode as discussed earlier, which in turn reduces convergence of electrical flux, thus contracting region I.

Marginal stability

We have seen in the previous section that, at large enough separator moduli (region IV in Fig. 4), the deposition-induced pressure gradient in the separator can reverse preferential deposition by creating a chemical potential gradient that drives depositing ions away from the perturbation tips. We also noted that this reversal occurs at all wave numbers and therefore can stabilize deposition of all modes. This motivates a detailed search for the criteria for marginal stability—the boundary in parameter space beyond which the deposition is stable for all perturbations. As stated earlier, marginal stability occurs at separator moduli high enough such that surface tension is negligible. Ignoring surface tension in Eqs. 26 to 28, $Z_1^{\mathrm{m}*}$ and $Z_1^{\mathrm{s}*}$ are both proportional to k^*. This implies that the first two terms of Eqs. 25 and 29 are proportional to k^*, whereas the third term goes as k^{*2}. As a result, in the relative competition of the corresponding mechanisms over various modes, we may expect the concentration of current density and separator compression to compete equally at all modes, whereas the electrode stress–driven changes in deposition rate can suppress instabilities above a certain k^* value.

Thus, high wave number perturbations are rendered stable by the retardation of the interfacial reaction by electrode pressure, arising from the elastic deformation of the separator and surface tension on tips in both low and high current densities. Therefore, marginal stability is achieved when deposition at small wave numbers is stabilized. This gives a relation between the three parameters [the fraction of immobilized anions ($C_{\mathrm{a,f0}}$), the elasto-osmotic number (Eo), and the electrical-elastic number (Ee)] or in dimensional terms [the fraction of immobilized anions ($C_{\mathrm{a,f0}}$), the separator modulus (G^{s}), and the current density (J)] for the boundary beyond which the deposition is universally stable. This relation can be determined by setting $\sigma_{\mathrm{mu}} = 0$ for both large and small current densities.

For small current densities, the marginal stability limit can be obtained from Eqs. 26 to 29 as

$$1 + \frac{1}{4} K^{\mathrm{s}*}\,\mathrm{Eo}\,\frac{Z_1^{\mathrm{s}*}}{k^*} = 0 \tag{35}$$

where $Z_1^{\mathrm{s}*}$ is given by

$$\frac{Z_1^{\mathrm{s}*}}{k^*} = \frac{2}{1+\alpha^{\mathrm{s}}} \left[\frac{\left\{\frac{1}{1+\alpha^{\mathrm{s}}} + \frac{G-1}{1+2\alpha^{\mathrm{s}}}\right\}\left\{(1+\alpha^{\mathrm{m}})(1-V) - (1+V)(1+\alpha^{\mathrm{m}}+\alpha^{\mathrm{m}}G)\right\}}{\left(\frac{1+2\alpha^{\mathrm{m}}}{1+2\alpha^{\mathrm{s}}}G + \frac{1+\alpha^{\mathrm{m}}}{1+\alpha^{\mathrm{s}}}\right)(1-V) - (1+\alpha^{\mathrm{m}}+\alpha^{\mathrm{m}}G)\left(\frac{2(G-V)}{1+2\alpha^{\mathrm{s}}} + \frac{1+V}{1+\alpha^{\mathrm{s}}}\right)} - 1 \right] \tag{36}$$

One can see from the above set of equations that the marginal stability criterion at small current densities is independent of Ee and $C_{\mathrm{a,f0}}$ and attained for Eo > 2.32 or $G^{\mathrm{s}} > 34$ MPa for the set of parameter values mentioned earlier. At this critical separator modulus, the concentration of ambipolar diffusion on the tips is counterbalanced by the pressure-driven flux away from the tips. Because ambipolar diffusion is independent of the fixed anions, the critical Eo value is independent of $C_{\mathrm{a,f0}}$. The pressure-driven flux also being proportional to J makes the criterion independent of Ee and J. The marginal stability is thus attained for a separator modulus of the same order as the osmotic pressure of the solution, which is much smaller than the modulus of the metal in most cases. It is hence useful to simplify Eq. 36 in the case of $G^{\mathrm{s}} << G^{\mathrm{m}}$, that is, $G >> 1$, which yields the marginal stability criterion as

$$\mathrm{Eo} = \frac{G^{\mathrm{s}}(\nu_{\mathrm{c}} + \nu_{\mathrm{a,m}})}{RT} \approx \frac{3}{1-V}\frac{3-4\nu^{\mathrm{s}}}{1+\nu^{\mathrm{s}}} \tag{37}$$

The critical G^{s} or Eo value is sensitive to the partial molar volumes of both ions, as well as the separator Poisson ratio, as can be seen from Fig. 5B. It is, however, independent of the electrode's modulus and Poisson ratio because the electrode is rigid compared to the separator and does not deform.

The marginal stability criterion at large current densities depends on all three parameters, namely, $C_{\mathrm{a,f0}}$, Eo, and Ee. In this regime, the pressure gradient–driven flux is destabilizing in the migration region because of its role in the migration region where it increases the concentration of the fixed salt in high-pressure locations. In the diffusion

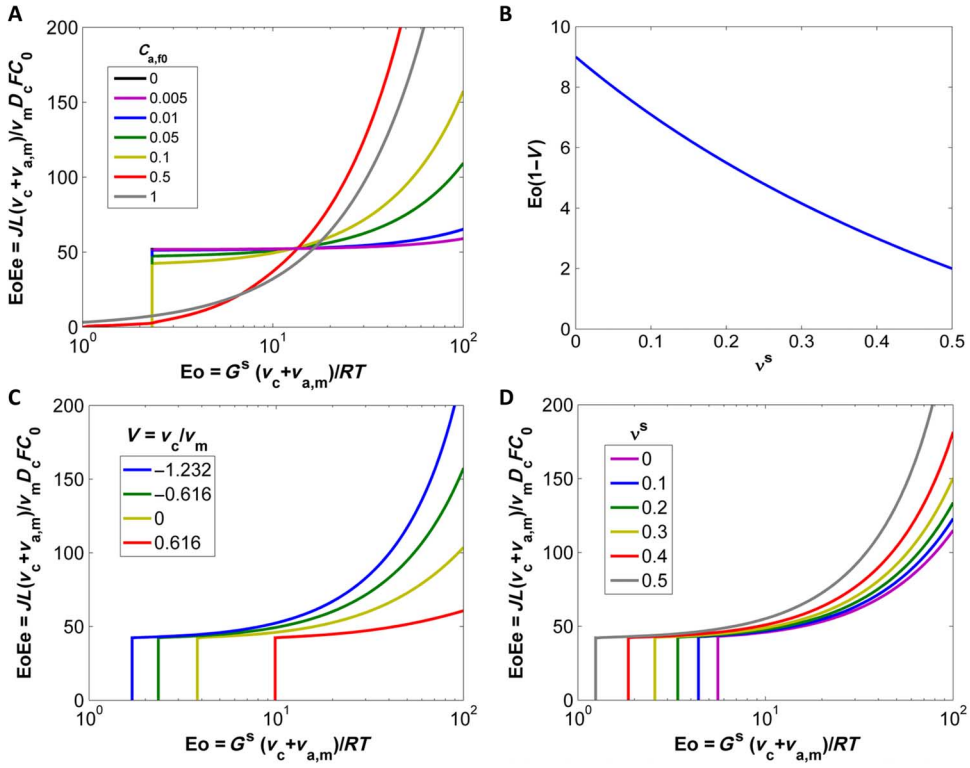

Fig. 5. Marginal stability of deposition. Relation between separator modulus and current density at varying fixed anion fractions for which the deposition is stable for all modes. (**A**) Marginal stability result for all current densities for parameter values mentioned in the paper. The deposition is fully stable at any point to the right of the corresponding curve. (**B**) Critical value of Eo at small current densities as a function of the separator Poisson ratio. (**C**) Marginal stability curves for $C_{a,f0} = 0.1$ and $\nu^s = 0.33$ for various values of cation partial molar volume. The partial molar volumes of the mobile anion ($v_{a,m}$) and the metal (v_m) are held constant at 1.78×10^{-4} and 1.3×10^{-5} m^3/mol, respectively. (**D**) Marginal stability for $C_{a,f0} = 0.1$, $v_c = -8 \times 10^{-6}$ m^3/mol, $v_{a,m} = 1.78 \times 10^{-4}$ m^3/mol, and $v_m = 1.3 \times 10^{-5}$ m^3/mol for various values of separator Poisson ratio.

region, the pressure gradient–driven flux is stabilizing as in the low–current density case. This makes the nature of its total effect dependent on the size of the migration region l^* as seen in the last term in Eq. 25, which varies as $k^*\exp(-2k^*l^*)$. That is, the destabilizing role of pressure-driven flux in the finite sized migration region is important for modes of wave number of the order of $1/l^*$ and attenuated when $k^*l^* << 1$. As we move toward higher k^* values, that is, $k^*l^* \geq 1$, the role of the migration region becomes more significant, and the stabilizing effect of pressure-driven flux in the diffusion region diminishes. For large k^* values, stability is obtained from elasticity-slowed reaction at the tips. Under the critical conditions, the migration region is small enough that the destabilizing contribution of the pressure-driven flux component and the concentration of electric field–driven flux on tips is counterbalanced by the effect of elasticity-slowed reaction kinetics and the stabilizing pressure-driven flux in the diffusion region. For separator moduli higher than this limit or current densities below it, the deposition is stable for all perturbation modes. As the elasticity-slowed reaction kinetics mechanism gains relative importance and the role of the finite size of migration region loses significance at higher k^* values, the marginal stability at high J occurs upon stabilization of a finite wave number $k_f^* = O(1/l^*)$ perturbation, which is the final mode to be stabilized. This argument suggests that under the critical conditions, the last mode to be stabilized is the most unstable mode and the critical mode at the same time. That is, $k_f^* = k_{cr}^* = k_{mu}^*$. Substituting this result in Eqs. 25 to 28, we obtain the following expressions, which can be solved simultaneously to obtain the relation between $C_{a,f0}$, G^s, and J for marginal stability.

$$1 - \frac{1}{2}\frac{Z_1^{s*}}{k_f^*} - \frac{1}{Ee}K^{m*}C_{a,f0}Z_1^{m*} + \frac{1}{4}(2 + K^{s*}\,Eo)\frac{Z_1^{s*}}{k_f^*}\exp\left(-2k_f^*l^*\right) = 0 \tag{38}$$

$$\frac{1}{Ee}K^{m*}C_{a,f0}Z_1^{m*} + \frac{1}{2}l^*(2 + K^{s*}\,Eo)Z_1^{s*}\exp\left(-2k_f^*l^*\right) = 0 \tag{39}$$

$$\frac{Z_1^{m*}}{k_f^*G} = \frac{2(1-V)\left[\frac{1}{1+\alpha^s} - \frac{1-G}{1+2\alpha^s}\right]}{\left(\frac{1+2\alpha^m}{1+2\alpha^s}G + \frac{1+\alpha^m}{1+\alpha^s}\right)(1-V) - (1+\alpha^m+\alpha^mG)\left(\frac{2(G-V)}{1+2\alpha^s} + \frac{1+V}{1+\alpha^s}\right)} \tag{40}$$

$$\frac{Z_1^{s*}}{k_f^*} = \frac{2}{1+\alpha^s}\left[\frac{\left\{\frac{1}{1+\alpha^s} - \frac{1-G}{1+2\alpha^s}\right\}\{(1+\alpha^m)(1-V) - (1+V)(1+\alpha^m+\alpha^mG)\}}{\left(\frac{1+2\alpha^m}{1+2\alpha^s}G + \frac{1+\alpha^m}{1+\alpha^s}\right)(1-V) - (1+\alpha^m+\alpha^mG)\left(\frac{2(G-V)}{1+2\alpha^s} + \frac{1+V}{1+\alpha^s}\right)} - 1\right] \tag{41}$$

The marginal stability result is shown in Fig. 5A, where the deposition is fully stable for conditions to the right of a curve. We plot Ee·Eo on the y axis to make it independent of separator modulus, whereas Eo is shown on the x axis to make it dependent on separator modulus. At low current densities, we obtain that the criterion of marginal stability is independent of $C_{a,f0}$ and Ee·Eo, and is given by a fixed value of Eo. At high current densities, we see that the marginal stability depends on the three parameters—$C_{a,f0}$, Eo, and Ee—which shows that improving the separator modulus (Eo) or fraction of fixed anions ($C_{a,f0}$) can increase the range of stable current densities (Ee·Eo). Conversely, we can attain stability by reducing the value of Ee·Eo, which can be done by either reducing the current density or improving the cation diffusivity. The cation diffusivity can be obtained from conductivity measurements using the Nernst-Einstein relation. Typical values for cross-linked polyethylene glycol (PEG) electrolytes range from $D_c = 0.2 \times 10^{-7}$ to 1×10^{-7} cm^2/s (*14*, *15*). For the set of values mentioned earlier with $C_{a,f0} = 0.1$, $G^s = 180$ MPa, $D_c = 0.5 \times 10^{-7}$ cm^2/s, and $C_0 = 1$ M, we predict that current densities $J < 0.19$ mA/cm^2 should experience stable deposition.

DISCUSSION

We have developed a single framework that combines the effects of electrochemical and mechanical properties to evaluate the stability of electrodeposition. We have shown through a linear stability analysis that morphological instabilities in electrodeposition can be suppressed through the use of solid electrolytes/separators with immobilized anions. Contrary to the popular notion in the literature that dendrite suppression requires electrolyte moduli comparable to that of the metal (*12*, *13*), our analysis reveals that the improvement in stability for electrodeposition of metals such as lithium can be achieved even for modest separator moduli of tens to hundreds of megapascals, which may be attainable even with polymeric materials. This finding is shown to arise from consideration of transport-driven growth of electrode surface perturbations that are suppressed by the elasticity.

Additionally, we investigate the stabilizing role of the pressure gradient in driving the mobile ions in the interelectrode space through a chemical potential gradient. This mechanism is shown to stabilize all modes of deposition even for separator moduli much lower than that of the metal electrode. It provides a qualitative explanation for several recent experimental observations (*14*–*19*) where stabilization of lithium metal electrodes is achieved at moderate separator moduli.

At current densities above the diffusion limit, the critical modulus for stability is reduced by increasing the fraction of immobilized anions or by reducing the applied current density. This suggests that enhancing the efficiency of anion immobilization facilitates not only stable electrodeposition of a metal, but also deposition at higher current densities. For current densities below the diffusion limit, the critical modulus for stability is independent of the fraction of immobilized anions and current density.

It is important to point out that the critical modulus $G^s \sim RT\left[\left(1 - \nu_c/\nu_m\right)\left(\nu_c + \nu_{a,m}\right)\right]^{-1}$ is sensitive to the partial molar volumes of the cation (Fig. 5C) and the mobile anion in the separator, as well as the partial molar volume of the metal, which means that it is unlikely to be a universal value even for electrodeposition of lithium at a fixed temperature. This prediction for G^s, although easily understood—the term $1 - \nu_c/\nu_m$ determines the magnitude of pressure gradient created by the deformation, whereas the term $\nu_c + \nu_{a,m}$ is an indication of its relative significance in the chemical potential—underscores the need for experimental studies that allow measurement and control of the ionic partial molar volumes in solid electrolytes. The lack of these experiments is to an extent understandable because the mechanism of marginal stability described here has not been proposed before.

Our analysis suggests several potential strategies to mitigate rough electrodeposition of metals using solid electrolytes/separators. Primary among these approaches are immobilization of a fraction of the anions in the electrolyte, increasing the separator modulus and reducing the current density at which deposition occurs. In quantitative terms, we find that immobilizing even 10% of anions or increasing the modulus of a polymer separator to tens or hundreds of megapascals via cross-linking and other strategies can lead to significant improvements over conventional salt-based, liquid electrolytes. All three strategies lead to significant improvement in the range of length scales over which the electrodeposition is stable. Qualitative support for these conclusions can be found in experimental studies (*14*–*23*). Although some of these strategies have been considered in the literature, the present analysis provides additional insight into the factors that govern their influence, thus opening up design pathways for potential outside-the-box solutions. For example, as noted earlier, the modulus requirement can be lowered by increasing the partial molar volumes of the ions in the electrolyte. Using an elastic membrane separator with strong chemical interactions with the dissolved ions would induce large volume changes in the separator on dissolving the salt. The reduction in the critical separator modulus with increasing Poisson's ratio suggests that using a polymer separator with low crystallinity would also be beneficial in suppressing dendrite formation. The dependence of deposition stability on deposit size suggests that restricting the deposition to only stable length scales may be yet another strategy. This may be achieved by either nanostructuring the separator (*42*) or altering the electrode architecture (*43*). Although each of these strategies should be effective by themselves, using them in combination should enhance their efficacy.

Quantitative comparisons between our theoretical predictions and results from experiments would be helpful in refining the theory. However, such comparisons are not possible at present due to lack of systematic electrodeposition experiments in solid electrolytes for which data for ionic partial molar volumes, mechanical moduli, transport properties, and stability limits are available. It is nonetheless still possible to make orders of magnitude estimates in a few cases to facilitate comparison with experiments. The work by Pan *et al.* (*15*), for example, reports mechanical moduli, conductivity, lithium transference number (t_{Li+}), and stability limits for solid electrolytes based on cross-linked PEG doped with LiTFSI. A transition from unstable to completely stable Li deposition is reported to occur at an electrolyte shear modulus of 33.6 MPa ($t_{Li+} = 0.25$) and at current density below 0.3 mA/cm^2, which is comparable to what we would expect from the theory. Additionally, electrolytes containing immobilized anions have been synthesized and reported to show complete stability in the modulus range 100 to 200 MPa, which is again consistent with the values expected from theory (*35*, *37*). Although it is clear that more quantitative comparisons are required to assess the theory reported here, we note that even the order of magnitude levels of agreement apparent from these limited comparisons are a significant improvement over previous work (*12*), which predicts that moduli in excess of 6 GPa are required to obtain stable electrodeposition of Li.

Electrodeposition of highly reactive metals such as lithium and sodium is significantly influenced by the presence of a passivation layer, called the SEI, on the metal surface (*10*, *11*), which forms because of reaction between the metal and the electrolyte. Although the SEI is not explicitly modeled here, the influence of the surface is phenomenologically represented by the surface tension. The value of the surface tension depends on the transport properties of ions in the SEI, elastic modulus of the SEI, and the interfacial tensions of the metal-SEI and SEI-electrolyte interfaces. Additives in the electrolyte are known to modify the nature of the SEI, which is thus captured in the present model as changes to the surface tension γ. Additives that increase the surface tension through SEI control improve the stability of deposition (*9*, *44*). A number of recent studies also attempt to stabilize the deposition by artificially designing the structure and chemistry of the SEI. Such studies would benefit from the guiding principles provided by the above analysis. Experiments that use thin coatings of single-ion conductors (*35*) or thin elastic layers of cross-linked polymer nanocomposites (*17*) on lithium metal surfaces find significant improvement in the stability of deposition. Although the low thickness of these layers thwarts quantitative comparison with the present study, the general principles by which elastic stresses and fixed anions enhance stability are still applicable for providing qualitative guidance of materials design.

MATERIALS AND METHODS

Following Mullins and Sekerka (*3*), we modeled the stability of deposition by considering the transport and deformation for planar electrodes, called the "base state," followed by perturbing the metal surface sinusoidally with small-amplitude perturbations, which would represent the various Fourier modes of surface corrugations, referred to as the "perturbed state." The motivation for this may be understood as follows. Any given electrode surface profile can be expressed as a Fourier series. For short times, the growth of each mode was decoupled from other modes (*3*). This implied that each mode can be analyzed separately and the linearity of the equations yielded that the growth of the full interface was simply given by the superposition of the growth of its component modes.

We present a short demonstration of the methodology of deriving the governing equations for transport and separator pressure in the low–current density case. The governing equations at high current densities and the boundary conditions were obtained through a similar process. The full set of equations is provided in the Supplementary Materials. Ignoring the contribution of the fixed anions at low current densities (*25*), Eqs. 3, 4, 8, and 9 can be simplified to

$$\nabla^2 C_c + \frac{\nu_c + \nu_{a,m}}{2RT}\nabla C_c \cdot \nabla p^s = 0 \tag{42}$$

$$\nabla^2 p^s = 0 \tag{43}$$

This set was satisfied by the base state fields C_c and p^s and in the perturbed state by the fields $\tilde{C}_c = C_c + \varepsilon C_c'(z)e^{\sigma t}e^{ikx}$ and $\tilde{p}^s = p^s + \varepsilon p^{s'}(z)e^{\sigma t}e^{ikx}$.

Base state

We started by solving the transport and deformation equations for planar, parallel, semi-infinite electrodes, with all deformations and fluxes in the z direction, normal to the electrodes. In this case, we found that the pressure gradient terms in the transport equations vanished, because pressure in the separator was uniform, that is, $\nabla p^s = 0$. Equation 42 gives $C_c = C_0\,(1 - C_{a,f0}) + J\,(2z - L)/(4D_cF)$, as shown in our previous paper (*27*) and in Fig. 1B.

Perturbed state

In the perturbed state, small-amplitude sinusoidal undulations were imposed on the metal surface. For perturbations of infinitesimal amplitudes, the concentration $[\tilde{C}_c = C_c + \varepsilon C_c'(z)e^{\sigma t}e^{ikx}]$ and pressure field $[\tilde{p}^s = p^s + \varepsilon p^{s'}(z)e^{\sigma t}e^{ikx}]$ were also expected to vary in the same manner (*3*), with the perturbation terms C_c' and $p^{s\prime}$ being allowed to take complex values to represent any out-of-phase behavior. The other fields in the problem not explicitly treated here, namely, potential, current density, and the deformation fields in the separator and the electrode, were also perturbed in a regular fashion. The amplitudes of the perturbations grew with time if the real part of σ was positive, which implied unsteady electrodeposition leading to dendritic structures. Because $\tilde{C}_c$ and $\tilde{p}^s$ satisfied Eqs. 42 and 43, we obtained

$$\nabla^2 \tilde{C}_c + \frac{\nu_c + \nu_{a,m}}{2RT}\nabla \tilde{C}_c \cdot \nabla \tilde{p}^s = 0 \tag{44}$$

$$\nabla^2 \tilde{p}^s = 0 \tag{45}$$

Substituting from $\tilde{C}_c = C_c + \varepsilon C_c'(z)e^{\sigma t}e^{ikx}$ and $\tilde{p}^s = p^s + \varepsilon p^{s'}(z)e^{\sigma t}e^{ikx}$, while using $\nabla p^s = 0$ as derived from the base state, we found

$$\nabla^2 C_c + \varepsilon e^{\sigma t}\nabla^2\left(C_c' e^{ikx}\right) + \frac{\nu_c + \nu_{a,m}}{2RT}\left[\varepsilon e^{\sigma t}\nabla C_c \cdot \nabla\left(p^{s'}e^{ikx}\right) + \varepsilon^2 e^{2\sigma t}\nabla\left(C_c' e^{ikx}\right)\cdot\nabla\left(p^{s'}e^{ikx}\right)\right] = 0 \tag{46}$$

$$\nabla^2 p^s + \varepsilon e^{\sigma t}\nabla^2\left(p^{s'}e^{ikx}\right) = 0 \tag{47}$$

Noting that the base state also satisfied the same governing equations, and the small value of ε implied $\varepsilon^2 << \varepsilon$, we obtained, on expanding the derivatives in terms of x and z, two governing equations for the perturbation fields C_c' and $p^{s\prime}$

$$\frac{d^2 C_{c'}}{dz^2} - k^2 C_{c'} + \frac{\nu_c + \nu_{a,m}}{2RT}\frac{dC_c}{dz}\frac{dp^{s'}}{dz} = 0 \tag{48}$$

$$\frac{d^2 p^{s'}}{dz^2} - k^2 p^{s'} = 0 \tag{49}$$

The boundary conditions were also obtained from a similar procedure, and the equations were concurrently solved to obtain the growth rate σ as a function of the wave number k and other system parameters. The wave number dependence may be summarized by considering the critical wave number k_{cr}, which defined the transition from stable to unstable deposition, and the growth rate of the least stable mode, which were defined as

$$\sigma(k_{cr}) = 0 \tag{50}$$

$$\sigma\left(\frac{d\sigma}{dk} = 0\right) = \sigma_{mu} \tag{51}$$

We also derived the conditions for marginal stability, that is, the relation between system parameters [separator modulus (G^s), fixed anion fraction ($C_{a,f0}$), and current density (J)] for which the growth rate was nonpositive for all modes ($\sigma \leq 0$ for all k), which gave the conditions for which the deposition was completely stable.

SUPPLEMENTARY MATERIALS

Supplementary material for this article is available at http://advances.sciencemag.org/cgi/content/full/2/7/e1600320/DC1

Perturbed equations at high current densities

Perturbed equations at low current densities

fig. S1. Critical wave number versus current density.

table S1. List of symbols, subscripts, and superscripts.

REFERENCES AND NOTES

1. M. Z. Bazant, Regulation of ramified electrochemical growth by a diffusive wave. *Phys. Rev. E* **52**, 1903–1914 (1995).
2. C. Léger, J. Elezgaray, F. Argoul, Dynamical characterization of one-dimensional stationary growth regimes in diffusion-limited electrodeposition process. *Phys. Rev. E* **58**, 7700–7709 (1998).
3. W. W. Mullins, R. F. Sekerka, Stability of a planar interface during solidification of a dilute binary alloy. *J. Appl. Phys.* **35**, 444–451 (1964).
4. I. Golding, Y. Kozlovsky, I. Cohen, E. Ben-Jacob, Studies of bacterial branching growth using reaction–diffusion models for colonial development. *Physica A* **260**, 510–544 (1998).
5. H. Gao, W. D. Nix, Surface roughening of heteroepitaxial thin films. *Annu. Rev. Mater. Sci.* **29**, 173–209 (1999).
6. R. Aogaki, K. Kitazawa, Y. Kose, K. Fueki, Theory of powdered crystal formation in electrocrystallization—Occurrence of morphological instability at the electrode surface. *Electrochim. Acta* **25**, 965–972 (1980).
7. J. K. Stark, Y. Ding, P. A. Kohl, Dendrite-free electrodeposition and reoxidation of lithium-sodium alloy for metal-anode battery. *J. Electrochem. Soc.*, **158**, A1100–A1105 (2011).
8. L.-G. Sundstrom, F. H. Bark, On morphological instability during electrodeposition with a stagnant binary electrolyte. *Electrochim. Acta* **40**, 599–614 (1995).
9. D. P. Barkey, R. H. Muller, C. W. Tobias, Roughness development in metal electrodeposition II. Stability theory. *J. Electrochem. Soc.* **136**, 2207–2214 (1989).
10. K. Xu, Nonaqueous liquid electrolytes for lithium-based rechargeable batteries. *Chem. Rev.* **104**, 4303–4417 (2004).
11. W. Xu, J. Wang, F. Ding, X. Chen, E. Nasybulin, Y. Zhang, J.-G. Zhang, Lithium metal anodes for rechargeable batteries. *Energy Environ. Sci.* **7**, 513–537 (2014).
12. C. Monroe, J. Newman, The impact of elastic deformation on deposition kinetics at lithium/polymer interfaces. *J. Electrochem. Soc.* **152**, A396–A404 (2005).
13. G. M. Stone, S. A. Mullin, A. A. Teran, D. T. Hallinan Jr., A. M. Minor, A. Hexemer, N. P. Balsara, Resolution of the modulus versus adhesion dilemma in solid polymer electrolytes for rechargeable lithium metal batteries. *J. Electrochem. Soc.* **159**, A222–A227 (2012).
14. R. Khurana, J. L. Schaefer, L. A. Archer, G. W. Coates, Suppression of lithium dendrite growth using cross-linked polyethylene/poly(ethylene oxide) electrolytes: A new approach for practical lithium-metal polymer batteries. *J. Am. Chem. Soc.* **136**, 7395–7402 (2014).
15. Q. Pan, D. M. Smith, H. Qi, S. Wang, C. Y. Li, Hybrid electrolytes with controlled network structures for lithium metal batteries. *Adv. Mater.* **27**, 5995–6001 (2015).
16. Y. Ansari, B. Guo, J. H. Cho, K. Park, J. Song, C. J. Ellison, J. B. Goodenough, Low-cost, dendrite blocking polymer-Sb_2O_3 separators for lithium and sodium batteries. *J. Electrochem. Soc.* **161**, A1655–A1661 (2014).
17. S. Choudhury, R. Mangal, A. Agrawal, L. A. Archer, A highly reversible room-temperature lithium metal battery based on crosslinked hairy nanoparticles. *Nat. Commun.* **6**, 10101 (2015).
18. I. Gurevitch, R. Buonsanti, A. A. Teran, B. Gludovatz, R. O. Ritchie, J. Cabana, N. P. Balsara, Nanocomposites of titanium dioxide and polystyrene-poly(ethylene oxide) block copolymer as solid-state electrolytes for lithium metal batteries. *J. Electrochem. Soc.* **160**, A1611–A1617 (2013).
19. S.-O. Tung, S. Ho, M. Yang, R. Zhang, N. A. Kotov, A dendrite-suppressing composite ion conductor from aramid nanofibres. *Nat. Commun.* **6**, 6152 (2015).
20. J. L. Barton, J. O'M. Bockris, The electrolytic growth of dendrites from ionic solutions. *Proc. R. Soc. Lond. A* **268**, 485–505 (1962).
21. O. Crowther, A. C. West, Effect of electrolyte composition on lithium dendrite growth. *J. Electrochem. Soc.* **155**, A806–A811 (2008).
22. C. Brissot, M. Rosso, J.-N. Chazalviel, S. Lascaud, Dendritic growth mechanisms in lithium/polymer cells. *J. Power Sources* **81–82**, 925–929 (1999).
23. T. Osaka, T. Homma, T. Momma, H. Yarimizu, In situ observation of lithium deposition processes in solid polymer and gel electrolytes. *J. Electroanal. Chem.* **421**, 153–156 (1997).
24. J.-N. Chazalviel, Electrochemical aspects of the generation of ramified metallic electrodeposits. *Phys. Rev. A* **42**, 7355–7367 (1990).
25. W. H. Smyrl, J. Newman, Double layer structure at the limiting current. *Trans. Faraday Soc.* **63**, 207–216 (1967).
26. K. T. Chu, M. Z. Bazant, Electrochemical thin films at and above the classical limiting current. *SIAM J. Appl. Math.* **65**, 1485–1505 (2005).
27. M. D. Tikekar, L. A. Archer, D. L. Koch, Stability analysis of electrodeposition across a structured electrolyte with immobilized anions. *J. Electrochem. Soc.* **161**, A847–A855 (2014).
28. I. Rubinshtein, B. Zaltzman, J. Pretz, C. Linder, Experimental verification of the electroosmotic mechanism of overlimiting conductance through a cation exchange electrodialysis membrane. *Russ. J. Electrochem.*, **38**, 853–863 (2002).
29. J. G. Wijmans, R. W. Baker, The solution-diffusion model: A review. *J. Membr. Sci.* **107**, 1–21 (1995).
30. R. J. Charles, Stress induced binary diffusion in a solid. *J. Electrochem. Soc.* **116**, 1514–1519 (1969).
31. N. Weber, M. Goldstein, Stress-induced migration and partial molar volume of sodium ions in glass. *J. Chem. Phys.* **41**, 2898–2901 (1964).
32. A. Mani, M. Z. Bazant, Deionization shocks in microstructures. *Phys. Rev. E* **84**, 061504 (2011).
33. Y. Marcus, G. Hefter, Standard partial molar volumes of electrolytes and ions in non-aqueous solvents. *Chem. Rev.* **104**, 3405–3452 (2004).
34. J. Song, H. Lee, M.-J. Choo, J.-K. Park, H.-T. Kim, Ionomer-liquid electrolyte hybrid ionic conductor for high cycling stability of lithium metal electrodes. *Sci. Rep.* **5**, 14458 (2015).
35. J. L. Schaefer, D. A. Yanga, L. A. Archer, High lithium transference number electrolytes via creation of 3-dimensional, charged, nanoporous networks from dense functionalized nanoparticle composites. *Chem. Mater.* **25**, 834–839 (2013).
36. Y. Lu, M. Tikekar, R. Mohanty, K. Hendrickson, L. Ma, L. A. Archer, Stable cycling of lithium metal batteries using high lithium transference number electrolytes. *Adv. Energy Mater.* **5**, 1402073 (2015).
37. G. H. McKinley, Dimensionless groups for understanding free surface flows of complex fluids. *Soc. Rheol. Bull.*, 6–9 (2005).
38. R. W. Style, J. S. Wettlaufer, E. R. Dufresne, Surface tension and the mechanics of liquid inclusions in compliant solids, *Soft Matter* **11**, 672–679 (2015).
39. R. W. Style, C. Hyland, R. Boltyanskiy, J. S. Wettlaufer, E. R. Dufresne, Surface tension and contact with soft elastic solids. *Nat. Commun.* **4**, 2728 (2013).
40. W. N. Bond, The surface tension of a moving water sheet. *Proc. Phys. Soc.* **47**, 549–558 (1935).
41. W. H. Hager, Wilfrid Noel Bond and the Bond number. *J. Hydraulics Res.* **50**, 3–9 (2012).
42. Z. Tu, Y. Kambe, Y. Lu, L. A. Archer, Nanoporous polymer-ceramic composite electrolytes for lithium metal batteries. *Adv. Energy Mater.* **4**, 1300654 (2014).
43. Q. Chen, K. Geng, K. Sieradzki, Prospects for dendrite-free cycling of Li metal batteries. *J. Electrochem. Soc.*, **162**, A2004–A2007 (2015).
44. J. J. Kelly, A. C. West, Copper deposition in the presence of polyethylene glycol. I. Quartz crystal microbalance study. *J. Electrochem. Soc.*, **145**, 3472–3476 (1998).

Acknowledgments: Funding: This material is based on work supported as part of the Energy Materials Center at Cornell, an Energy Frontier Research Center funded by the U.S. Department of Energy, Office of Science, Office of Basic Energy Sciences under Award Number DESC0001086. **Author contributions:** All authors contributed to the development of the model. M.D.T. solved the equations and made the figures. All authors wrote the article. **Competing interests:** L.A.A. is a founder and scientific advisor for NOHMs Technologies, which is focused on commercializing electrolytes and electrodes for lithium-sulfur and lithium-ion batteries. **Data and materials availability:** All data needed to evaluate the conclusions in the paper are present in the paper and/or the Supplementary Materials. Additional data related to this paper may be requested from the authors.

Submitted 11 February 2016
Accepted 16 June 2016
Published 15 July 2016
10.1126/sciadv.1600320

Citation: M. D. Tikekar, L. A. Archer, D. L. Koch, Stabilizing electrodeposition in elastic solid electrolytes containing immobilized anions. *Sci. Adv.* **2**, e1600320 (2016).

Stabilizing electrodeposition in elastic solid electrolytes containing immobilized anions

Mukul D. Tikekar, Lynden A. Archer and Donald L. Koch

Sci Adv **2** (7), e1600320.
DOI: 10.1126/sciadv.1600320